Molecular dynamics simulation studies of atomic-level structures in rapidly quenched Ag-Cu nonequilibrium alloys

H. W. Sheng, J. H. He, and E. Ma*

Department of Materials Science and Engineering, The Johns Hopkins University, Baltimore, Maryland 21209
(Received 11 December 2001; published 19 April 2002)

Ag-Cu has been a classical example demonstrating the formation of a single-phase supersaturated solid solution by rapid quenching in a system immiscible in equilibrium at room temperature. This study examines, using molecular dynamics simulations, the local structures and homogeneity of these crystalline and amorphous Ag-Cu alloys produced by quenching from the liquid at different cooling rates ($5 \times 10^{10} - 2.5 \times 10^{13}$ K/s). It is observed that the retention of amorphous structures requires extremely high quench rates. The amorphous alloys formed are chemically uniform in both long and short ranges. Meanwhile, topologically significant local icosahedral order was able to develop during quenching even at these extreme cooling rates. The Ag-Cu amorphous structures are discussed in comparison with those of Ag-Ni, a system immiscible even in the liquid state. At moderately reduced quench rates, homogeneous crystalline solutions form instead. With further decreasing quench rates, the chemical short-range-order parameter becomes increasingly more positive, suggesting spinodal decomposition. Our simulations point to the need for a careful experimental study of the ultrafine-scale composition modulations in the face-centered-cubic solid solution that is hitherto believed to be homogeneously supersaturated for a wide range of rapid-quench conditions.

I. INTRODUCTION

The eutectic Ag-Cu system is one of the many binary systems with a positive heat of mixing (positive ΔH) in both the solid and liquid states.[1,2] In the equilibrium phase diagram the two elements are soluble in the liquid state due to the large entropic contributions to the free energy of mixing at high temperatures, but exhibit practically no mutual solubility near the ambient temperature.[1,2] Over the past several decades, there have been a large number of publications reporting that solid-solution alloys can be created in this system through processing under far-from-equilibrium conditions.[3–18] In fact, the formation of a continuous series of fcc Ag-Cu solid solutions, and occasionally amorphous Ag-Cu alloys, was one of the earliest demonstrations of nonequilibrium alloy formation by rapid quenching from the liquid[3–5] or vapor phases.[6–10] Since the early 1960's, there has been an increasing number of claims of new alloys in systems with positive ΔH,[19–28] such as Cu-Co, Cu-Cr, Cu-Fe, Ag-Cu, and sometimes even in systems that exhibit a large miscibility gap in the liquid state, such as Cu-Ta, Cu-Nb, Cu-W, Ag-Ni, Ag-Co, and Ag-Fe. Typical processing techniques employed to achieve alloying include vapor deposition through evaporation and sputtering,[6–10,17,18] melt quenching,[3–5] ion beam mixing,[11,12] and mechanical alloying.[13–16]

The nonequilibrium alloys created in such positive ΔH systems are interesting because their formation has to survive a thermodynamic driving force for phase decomposition. As a result, in contrast to systems with a negative ΔH that drives spontaneous intermixing, true atomic-level alloying and the chemical homogeneity of the two constituent elements cannot be taken for granted. Unfortunately, for the vast majority of previous experiments only diffraction methods were used to prove the formation, and characterize the structure, of the new alloys. The possibility of overlap between broad diffraction peaks when crystal and domain sizes are extremely small makes it difficult to ascertain if a single-phase homogeneous alloy is formed[28] or to distinguish between a mixture of nanocrystalline grains/domains and a truly amorphous structure.[29] Moreover, the development of short- to medium-range clustering, or any other types of local chemical or topological structures, remains unexplored so far. In comparison, it has been uncovered for many years that the short-range chemical ordering and topological local order in the conventional negative ΔH amorphous alloys are extremely important to their metastability.[30–33] For the crystalline solutions, it has been modeled recently that a decomposed microstructure, when coherent or semicoherent on the nanometer scale as in incipient spinodal decomposition, can in itself also lead to a single set of Bragg peaks appearing at the positions corresponding to the average lattice parameter of the two elements, close to that of a truly homogeneous supersaturated solution.[28] As an example, a recent high-resolution microstructure analysis of Cu-Co solid solutions prepared by melt spinning[23,24] and room-temperature cosputtering[28] indeed proved that spinodal decomposition was actually not suppressed for compositions near the center of the phase diagram due to the positive ΔH in this system as the driving force for phase separation.

It is therefore of interest to examine in detail the atomic-level structures of the unstable phases formed in positive ΔH systems to understand exactly what kind of alloys can be, and have been, created. Several issues regarding the nonequilibrium Ag-Cu alloys will be addressed in this paper. First of all, we will explore under what rapid quenching conditions the amorphous alloys and fcc solid solutions form, respectively, to explain the seemingly conflicting claims in the lit-

erature of the appearance of both phases. Second, the nature of the atomic-level structure of the amorphous Ag-Cu alloys formed will be monitored. Specifically, we will probe into the chemical and topological short-range order developed at different stages of quenching. The results will be compared with those of amorphous Ag-Ni, a system with a larger positive ΔH and immiscible in both liquid and solid states,[34–36] and with local structures developed in negative ΔH alloys. Third, for the repeatedly reported fcc Ag-Cu alloys, generally presumed to be homogeneous supersaturated solid solutions based on simple diffraction results, we will examine the possibility that the solutions are not really random and homogeneous and determine the extent of the nonuniformity developed during quenching due to incipient phase separation on extremely fine (nanometer) scales.

Molecular dynamics (MD) simulation is used in this work. MD modeling is very useful, and sometimes indispensable, for tackling the challenging tasks listed in the last paragraph. MD simulations can provide details of the local structures that are difficult to access in laboratory experiments.[37–41] MD also captures the structural development in different stages of quenching. The cooling rates used for MD simulations can be similar to or beyond what is achievable in laboratory rapid quenching experiments. The MD results may thus provide insight into the local structural features and the corresponding thermodynamic properties possibly present in experimental alloys under various quenching conditions. For Ag-Cu, reliable interatomic potentials are available,[42] so that a comparison of the MD results with the experimentally determined structures and enthalpies is possible (a detailed experimental study is beyond the scope of this paper and will be reported in a forthcoming publication).

II. SIMULATION METHOD

MD simulations were performed at zero pressure with the Gibbs ensemble (N-P-T) implemented using the Parrinello-Rahman algorithm[43] to control the pressure and the Nosé-Hoover method[44] to control the system temperature. Tests with the Wentzcovitch algorithm[45(a)] produced similar results. Equations of motion were numerically integrated using the fifth-order Gear predictor-corrector method[45(b)] with a time step of 2 fs. Each simulation box has up to 2000 atoms at the desired composition, under periodic boundary conditions. The initial velocities of atoms follow the Boltzmann distribution at the desired temperature. The enthalpy of the system was determined by summing up the potential and kinetic contributions. For each quench experiment, the starting liquid state was obtained by heating the solid slowly through the liquidus temperature. The system was melted and homogenized at a temperature well above the liquidus in the range of 1250–1500 K for 100 ps and then rapidly cooled with the desired rate (e.g., at 5×10^{13} K/s or 0.1° per time step) down to room temperature.

Since we are interested in the behavior of both the fcc solution and the undercooled liquid that evolves into the amorphous phase through glass transition, an appropriate Ag-Cu interaction potential must be chosen and validated for both phases. Our prior experience indicates that an embedded atom method (EAM) potential is adequate for describing the behavior of the crystalline Ag-Cu phases including the fcc solid solution.[14,46] It does not, however, reproduce the experimentally measured heat of mixing in the liquid.[2] On the other hand, the tight-binding Ag-Cu potential of Mozzone *et al.*[47] reproduces the liquid heat of mixing at high temperatures and is useful for simulating the liquid or undercooled liquid alloy.[48] But this latter potential predicts a positive ΔH much too large for the fcc solid solution when compared with recent experimental data.[49] The Sutton-Chen Ag-Cu potential,[42] after a minor modification, was found to be able to reproduce all the available heat of mixing data for both the fcc solid solution and the high-temperature liquid.[49] This potential will be used to model both phases in the central concentration range. A cutoff distance of 6.5 Å was chosen for the atomic interactions, corresponding up to the fifth coordination shell in fcc Ag.

Most of the results reported in this paper are for the slightly hypoeutectic composition of $Ag_{70}Cu_{30}$, as an example. Out of the several compositions we looked at in a preliminary survey, this composition is chosen for a systematic study because, compared with more concentrated (e.g., equiatomic) alloys, the kinetics are faster and the MD runs are thus more manageable in terms of simulation time. This allowed us to simulate at some fairly slow cooling rates and obtain both the amorphous and the crystalline solutions at this composition with a variety of local structures. The structures of the alloys obtained in MD are analyzed using the radial distribution function [(RDF), i.e., the pair distribution function $g(r)$], chemical short-range-order (CSRO) parameter, three-dimensional atomic configurations, and the common-neighbor analysis (CNA) method.

III. RESULTS

A. Amorphous solid solutions

1. Cooling rate dependence

Figure 1 shows the RDF's of $Ag_{70}Cu_{30}$ after quenching from the liquid at different cooling rates to 300 K. For high quench rates of 5×10^{12} K/s and above, discrete crystalline peaks are absent in the RDF's, suggesting amorphous or liquidlike structures. The split second peak in the RDF's is a feature frequently observed for amorphous materials.[50] The evolution of the enthalpy was monitored during the cooling process, and the results for several different quench rates are shown in Fig. 2. Again, for quench rates of 5×10^{12} K/s and above, the exothermic step associated with crystallization is absent during cooling. The glass transition temperature T_g can be determined by monitoring the thermodynamic properties[39,51] during undercooling. The point at which both the enthalpy and volume change slope is taken as the T_g. As shown in Fig. 3 as an example, T_g is 510 K for $Ag_{70}Cu_{30}$ at the cooling rate of 2.5×10^{13} K/s. This value is close to those of Qi *et al.* obtained for $Ag_{60}Cu_{40}$ by similar MD simulations.[51]

At lower quench rates of 2.5×10^{12} K/s and below, the quenched $Ag_{70}Cu_{30}$ alloys all exhibit crystalline features in
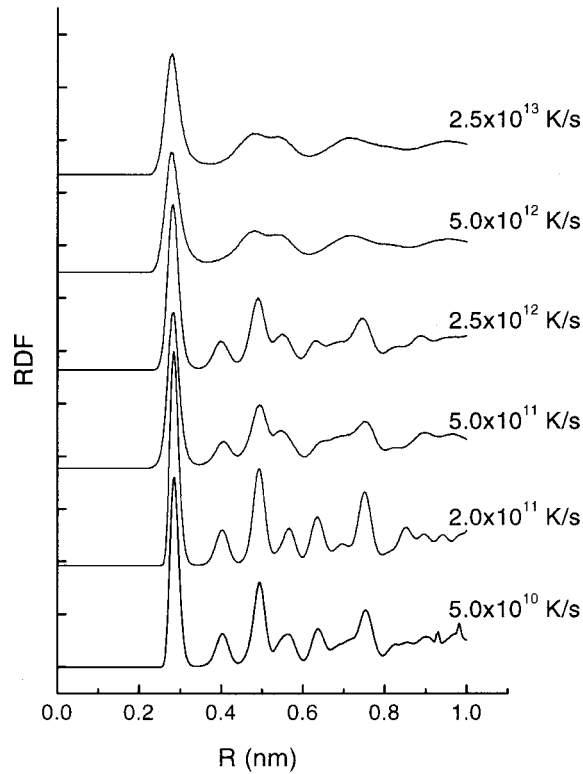
FIG. 1. Radical distribution functions of $Ag_{70}Cu_{30}$ quenched from liquid at different cooling rates, showing the formation of amorphous and crystalline solutions.

FIG. 2. Evolution of the enthalpy during quenching of $Ag_{70}Cu_{30}$ at the six different cooling rates.

their RDF's, Fig. 1. A heat of crystallization is associated with the crystallization of the undercooled liquid into the crystalline solution, seen in Fig. 2 as a stepwise downward jump. The crystalline solutions will be discussed in Sec. III B. Incidentally, for more concentrated alloys such as $Ag_{50}Cu_{50}$, the alloy remains amorphous at the quench rate of 2.5×10^{12} K/s due to slower atomic movements. As mentioned before, we will focus on a fixed composition of $Ag_{70}Cu_{30}$ to observe the wide range and trend of structural developments.

2. Chemical short-range-order parameter in the amorphous state

We now proceed to analyze the structural properties. The tendency for ordering or clustering can be characterized using the Warren-Cowley chemical CSRO parameter[52] defined as

$$CSRO = 1 - \frac{N_{AB}}{NC_B}, \qquad (1)$$

where N_{AB} is the nearest coordination number of B atoms around an A atom, N is the total coordination number in the nearest-neighbor shell, and C_B is the atomic concentration of B. Positive and negative CSRO parameter values indicate clustering and ordering, respectively. Figure 4 shows the evolution of the CSRO parameter during quenching at four different quench rates for $Ag_{70}Cu_{30}$. For the rapid cooling rate of 5×10^{12} K/s (and presumably any rate above this), the undercooled liquid amorphous alloy shows a CSRO param-
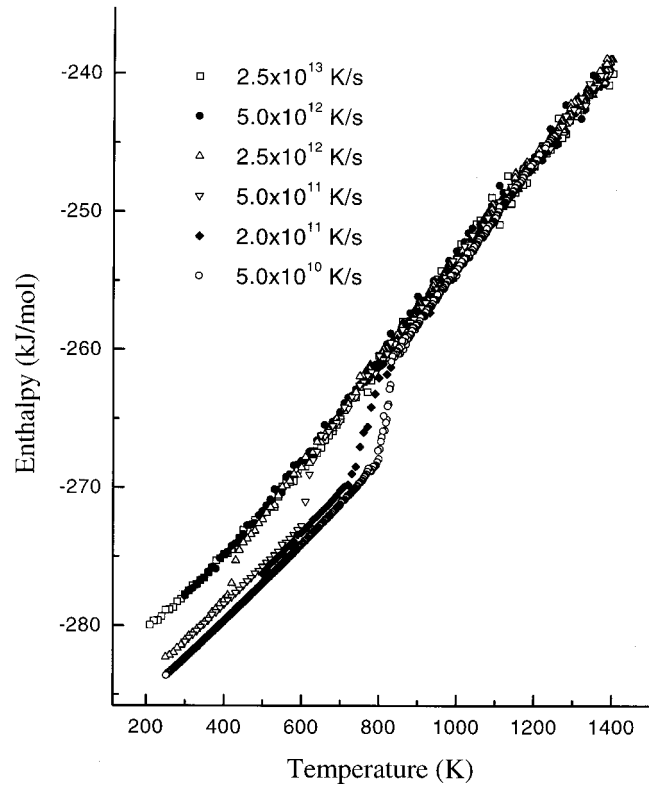
eter close to zero at all temperatures, indicating little decomposition during quenching. The alloy obtained can thus be regarded as a random amorphous solid solution. A projection of the amorphous structure is displayed in Fig. 5, in comparison with a crystalline structure obtained at a lower quench rate. The CSRO development in the crystalline solution at lower cooling rates will be discussed in Sec. III B.
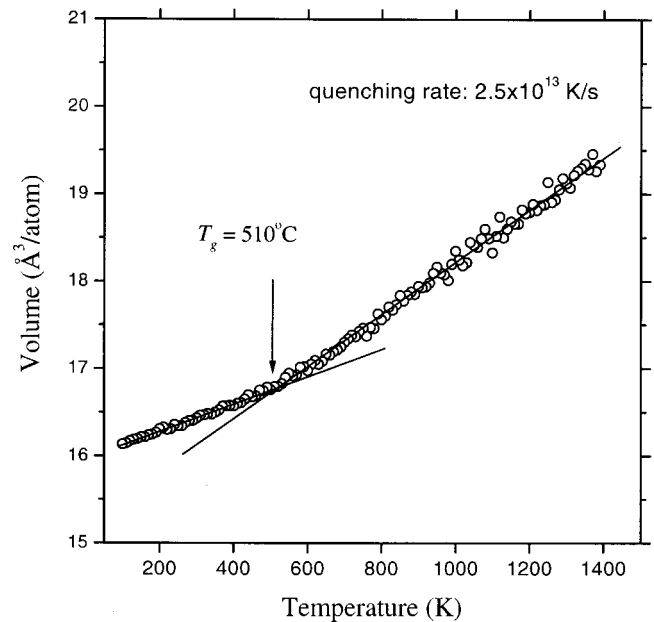

FIG. 3. Atomic volume changes slope at the glass transition temperature T_g, for $Ag_{70}Cu_{30}$ at the quench rate of 2.5×10^{13} K/s.
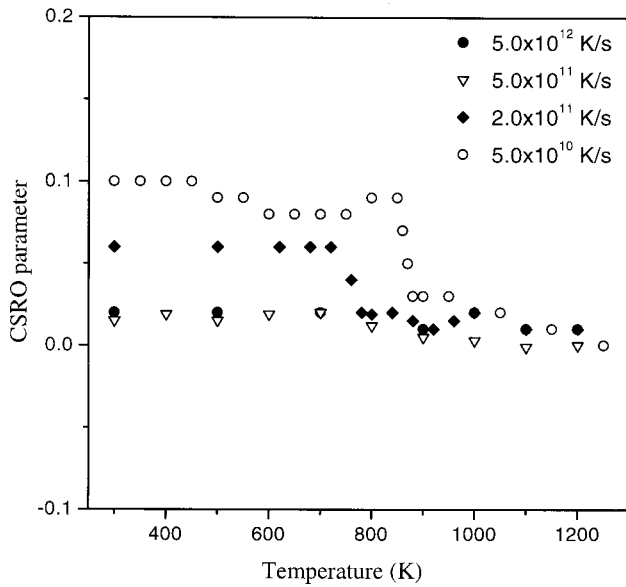
FIG. 4. CSRO parameter as a function of temperature during quenching at different rates. The final structure is amorphous at 5×10^{12} K/s, and those for the other three rates are crystalline.

3. Common-neighbor analysis of local icosahedral order in the amorphous solution

A number of simulations[37–41] have predicted short-range topological ordering based on icosahedral or distorted and fragmented icosahedral arrangements in elemental amorphous solids and binary amorphous alloys with negative ΔH. Experiments of metallic glasses have also detected the five-fold symmetry and icosahedral arrangements,[53,54] but mostly in systems where quasicrystalline alloys form. It is therefore of interest to examine whether icosahedral ordering also exists, and the degree of its development, in an amorphous alloy in a binary system such as Ag-Cu with a positive ΔH and no quasicrystal formation.

One instrument that can be used to analyze the local environments is the common-neighbor analysis (CNA).[37] The CNA is a method for analyzing structures by a decomposition of the RDF according to the local environment of the bonded pairs. The first RDF peak, for example, is composed of bonded nearest-neighbor pairs with different environments. Here the "bonded" nearest neighbors are those within the radius range from zero to a cutoff distance r_c, where r_c is taken as the position of the first minimum of the total RDF. Setting a different cutoff for each of the Ag-Ag, Ag-Cu, and Cu-Cu bond types is not necessary because the first minimum in the total RDF can be used to separate the nearest-neighbor bonds in all three partial RDF's. Each such bonded pair of atoms is systematically classified according to its surroundings in the following way: A set of three indices jkl specifies the local environment of the pair. The first index j is the number of neighbors common to both atoms. The second index k is the number of nearest-neighbor bonds between the common neighbors. The third index l is the number of bonds in the longest continuous chain formed by the k bonds between common neighbors. After each pair has been assigned to one of the various jkl types, a RDF $g_{jkl}(r)$ for each type of
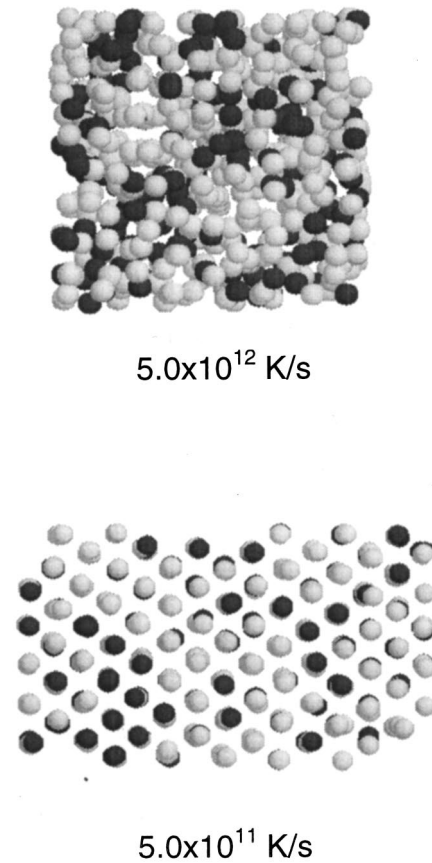

5.0x10^{12} K/s

5.0x10^{11} K/s

FIG. 5. Two-dimensional cross sectional projections of amorphous vs crystalline structures obtained at two different quench rates. Dark balls are Cu atoms.

the pairs can then be obtained and the total RDF is the summation of these pair RDF's.

The CNA can be used to distinguish between various local packing orders, in particular fcc, hcp, and icosahedral environments. Specifically, all bonded pairs in an icosahedron arrangement of 13 spheres are of type 555 because the central sphere forms a 555 pair with each of its 12 neighbors. If one bond is broken between a pair of outer spheres in an icosahedron, two of the 555 pairs get transformed into 544 pairs and two get transformed into 433 pairs.[36,37] This represents a type of distorted icosahedral order. In contrast, 421 and 422 pairs are characteristic of fcc and hcp order. The only bonded pairs in the fcc crystal are 421, while the hcp crystal has equal numbers of 421 and 422.[37]

Using the atomic positions stored for the Ag-Cu alloy during cooling, its RDF was decomposed into a set of RDF's, each for a specified jkl type. The seven major types of pairs (555, 433, 544, 421, 422, 311, and 666, others with populations less than 2% are neglected) for $Ag_{70}Cu_{30}$ are monitored during quenching. Figure 6 shows the normalized number, or the relative fraction, of the various CN pair types, as a function of temperature during a quench at 5×10^{12} K/s. For the amorphous alloy obtained, the 555 pair is apparently the most abundant and 433 and 544 pairs are second, indicating the dominance of icosahedral (including distorted icosahedral) order. Only small percentages of 422 pairs and 421 pairs are found, indicating that crystalline hcp
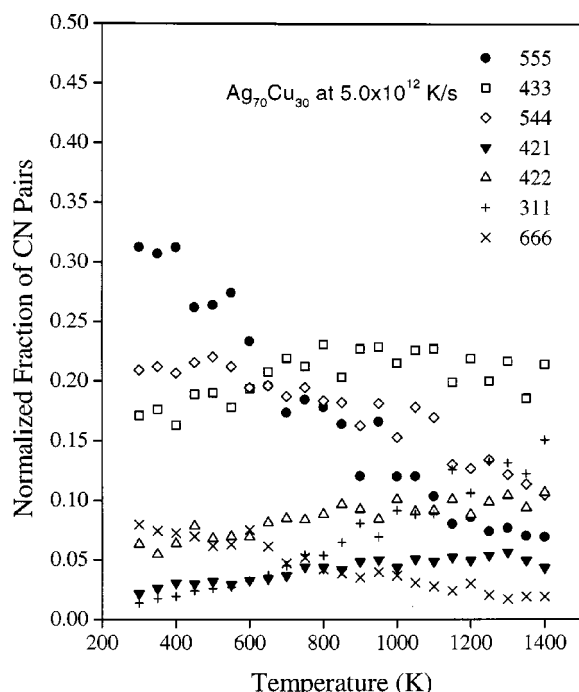
FIG. 6. Abundance of various common-neighbor (CN) pairs in (amorphous) $Ag_{70}Cu_{30}$ at different temperatures during quenching at 5×10^{12} K/s, showing the dominance of CN pairs characteristic of icosahedral local order.

FIG. 7. Abundance of various common-neighbor (CN) pairs in (fcc) $Ag_{70}Cu_{30}$ at different temperatures during quenching at 2×10^{11} K/s, showing the dominance of the 421 pairs characteristic of fcc local order in the product alloy.

and fcc local orders are insignificant. Dense random packing thus apparently also plays an important role in controlling the local topological order in these homogeneous Ag-Cu amorphous alloys with little chemical partitioning, contributing to the reduction in system energy. The predominance of the local icosahedral features over crystalline short-range packing can be viewed as a supporting evidence for the amorphous nature of the structure.

Figure 6 clearly indicates that there is a substantial and continuous increase of 555 pairs in the quenching process. The increase of 555 pairs representing the icosahedral ordering is a major contributor to an excess specific heat in the amorphous structure[30(b),36] and consequently the rate of enthalpy reduction during undercooling (Fig. 2). It is interesting that the local icosahedral order develops to such a high degree even though the quench rate is extremely high at 5×10^{12} K/s. Apparently, such local atomic arrangements require only very limited short-range diffusion. In addition, while 555 pairs increase in the quenching process, the population of 422 and 421 pairs (representing fcc and hcp) remains low in the entire quenching process, in sharp contrast to the dominant fcc local order in the crystallized solutions obtained at reduced quench rates, to be discussed in the following section (Fig. 7).

B. Crystalline solid solutions

As shown in Fig. 1, amorphous alloys can only be obtained at extremely high quench rates, at the high end of the effective quench rates achievable in laboratory vapo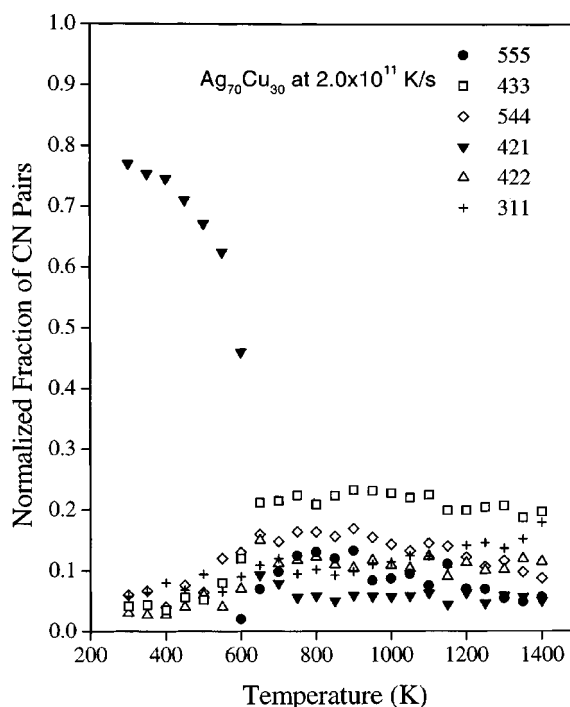r quenching experiments (usually estimated to be $\gtrsim 10^{10}$ K/s,[55] although a definitive determination is difficult). This is in agreement with experimental findings. In fact, the only two groups that produced amorphous rather than fcc Ag-Cu solutions employed procedures that are likely to yield the highest possible effective quench rates.[6–9] They used evaporation rather than sputtering so that the arriving particles have less kinetic energy, and it was found that the amorphous phase only appeared when the liquid-nitrogen-cooled substrate is a fast heat-conducting metal.[6–9] In all other quenching experiments from the vapor or liquid phase,[3–5,10,18] the product alloy is crystalline. This is consistent with the MD results of Figs. 1 and 2 for the more typical quench rates for deposition ($\lesssim 2.5\times10^{12}$ K/s).

As shown in Fig. 4 for $Ag_{70}Cu_{30}$, it is apparently possible to obtain a crystalline solution close to being homogeneous, as the CSRO parameter is practically constant and only slightly positive after the quench if a high cooling rate of 5×10^{11} K/s (or higher at 2.5×10^{12} K/s) is adopted. Chemical partitioning is largely suppressed at such quench rates, and the polymorphous crystallization is pushed to a fairly low temperature (Fig. 2). There are approaches that may possibly reach such high quench rates in laboratory experiments, e.g., by employing a low deposition rate to reduce substrate heating and a highly conductive and cold (e.g., cooled by liquid nitrogen or liquid helium) substrate. Considering the fact there have been a couple of reports of amorphous phase formation in Ag-Cu by vapor quenching, which requires even higher cooling rates (Sec. III A), a rate at or above 5×10^{11} K/s ought to be possible with carefully chosen deposition parameters.

(a)

2.0x10^{11} K/s

5.0x10^{10} K/s

(b)

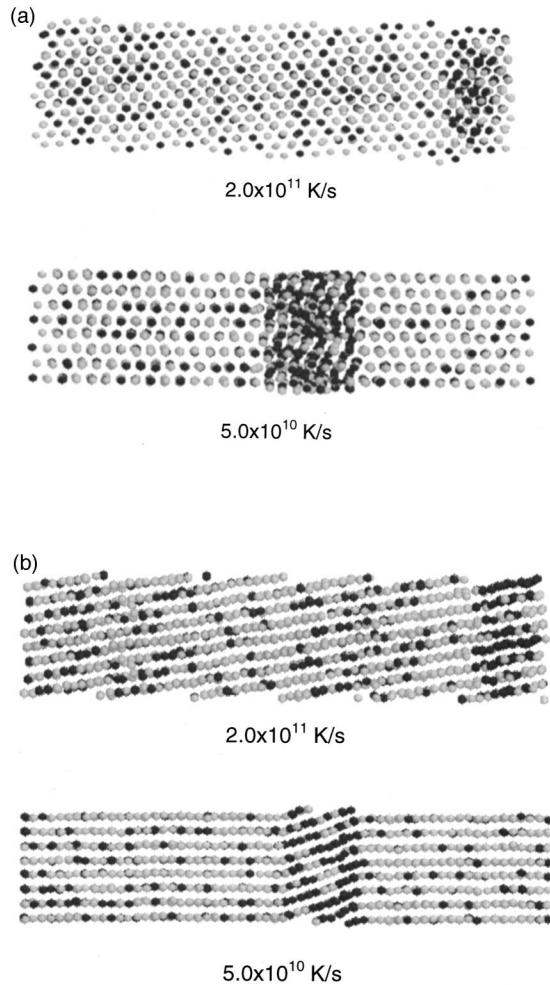2.0x10^{11} K/s

5.0x10^{10} K/s

FIG. 8. Two-dimensional cross-sectional projections of the crystalline structures obtained at the two slower quench rates in Fig. 4, showing the trend of increasing segregation. The views in (a) show the close-packed planes, while those in (b) reveal the structure of the regions with higher solute concentrations.

However, in many deposition experiments slower effective cooling rates of $<5\times10^{11}$ K/s are also likely. In this case, the positive CSRO parameters seen in Fig. 4 for the two lower quench rates (2×10^{11} and 5×10^{10} K/s) predict that there will be clustering and incipient phase decomposition inside the solution. Slowing down the quench also renders the crystallization of the undercooled liquid possible at higher temperatures, as shown in Fig. 2. At 2×10^{11} K/s, the CSRO parameter indicating local clustering rises over the same temperature range where crystallization of the undercooled liquid takes place, Fig. 2. Upon quenching at the even slower rate of 5×10^{10} K/s, the CSRO parameter increases in the undercooled liquid during cooling and jumps sharply at about 880–850 K (Fig. 4), a temperature similar to what is predicted for the critical temperature for the liquid miscibility gap using CALPHAD extrapolations[2] (see the next section). Crystallization sets in afterwards at a slightly lower temperature of 830 K.

Figures 5 and 8 compare the structure snapshots of the crystalline solutions discussed in the last two paragraphs.

Note that a clearer visualization would require a three-dimensional view with crystal rotations. However, some differences in terms of homogeneity can already be seen in these two-dimensional cross-sectional projections. For the two slower cooling rates (Fig. 8), the crystalline solutions exhibit clustering and nonuniformity. The bottom view in Fig. 8(b), from an angle different from the projections in Fig. 8(a), demonstrates that the region with higher solute concentration is not much more positionally disordered than the neighboring regions, but may be a result of coherent twining.[56] Figure 7 monitors the development of local topological order during quenching at 2×10^{11} K/s. It shows that while the six major pairs are of similar fractions in the high-temperature liquid as in the faster cooling case that resulted in the retention of amorphous alloy (Fig. 6), the local fcc order, in terms of the number of 421 pairs, jumps abruptly during crystallization at the expense of icosahedral order. After crystallization practically no 555 pairs are left, while the 421 pair reaches very high percentages, consistent with the final product being an fcc solid solution. Note that the fcc solution is indeed the predominant phase in laboratory quenching experiments under various conditions,[49] as identified based on diffraction results.

From the CSRO parameter in Fig. 4 and the atomic configurations shown in Fig. 8, we conclude that the solution is no longer homogeneous for the slower cooling rates employed in this study. Real-world quench experiments can have cooling rates even lower. For example, for melt quenching experiments the cooling rate is estimated to be as low as 10^6 K/s.[55] It would be interesting to examine the structural details of Ag-Cu solutions prepared using such quench rates. Unfortunately, MD solidification experiments with cooling rates slower than those used in this study are not practical given the limited MD simulation capabilities. For example, for a cooling rate of 10^9 K/s, it would require one microsecond to cover a temperature range of 1000 K during the quench. This is beyond the $\sim$10 ns time scale available to us in our MD runs. The possibilities of phase separation for much slower cooling rates will be discussed in the next section.

IV. DISCUSSION

A. Amorphous solutions

The absence of the development of appreciable clustering in the undercooled liquid/amorphous solution deserves a comment. Such a homogeneous alloy is expected only at high temperatures in the equilibrium liquid. The heat of mixing in the Ag-Cu liquid is positive, but relatively small [$+3.62$ kJ/mol at the equiatomic composition at 1423 K (Ref. 2)]. The relatively large entropy contribution at sufficiently high temperatures renders the free energy of mixing negative, and as a result, the Ag and Cu are homogeneously intermixed in the equilibrium liquid. At lower temperatures in the undercooled liquid, a metastable miscibility gap is possible. An estimate based on the extrapolation of the sub-regular solution model for the Ag-Cu liquid in Ref. 2 places the critical temperature for the liquid state miscibility gap at about 800 K. However, this temperature is fairly close to the

glass transition temperature of ~500 K (Fig. 3) where the undercooled liquid freezes into a glass, such that the temperature window favorable for phase decomposition is small in a rapid quench. As the amorphous phase is obtained at extremely rapid quench rates at or above ~5×10^{12} K/s, there is insufficient time for the undercooled liquid to catch the nose in the temperature-time-transformation (TTT) diagram to yield obvious phase separation. A homogeneous amorphous solution is obtained as a result, as demonstrated by the CSRO parameter in Fig. 4.

This scenario is very different from that observed in the amorphous structures in the Ag-Ni liquids quenched at similar cooling rates, where one observes spinodal-like phase separation features with modulation wavelengths of the order of one nanometer as well as a positive CSRO parameter as large as above 0.2.[34–36] This difficulty in bypassing (incipient) decomposition in the Ag-Ni case is clearly associated with the huge liquid miscibility gap due to the large magnitude of the positive ΔH. As seen in the Ag-Ni equilibrium phase diagram,[57] the liquid miscibility gap persists to very high temperatures. Again, using the CALPHAD approach the critical temperature for the liquid miscibility gap can be estimated to be as high as 2800 K.[58] As a consequence, there is driving force for phase separation over a wide range of temperatures in the liquid and undercooled liquid states during the quench, with sufficient time spent at temperatures where diffusion kinetics are sufficient for nanometer or subnanometer-scale segregation.

Note that in diffraction studies both the vapor-deposited amorphous Ag-Cu and Ag-Ni alloys exhibit similar diffused halos.[6–9,34–36] They would be considered similar positive ΔH amorphous alloys and presumed homogeneous considering the extremely rapid quench used to deposit them. But in actuality they are very different: one close to being truly homogeneous (Ag-Cu) and one undergone phase separation on a scale so fine that it could easily escape detection (Ag-Ni).

These amorphous alloys are also different from those obtained in easy glass-forming systems where strong short-range ordering to increase the number of unlike bonds is the norm due to the large negative ΔH. Phase separation and two-phase coexistence in the amorphous state are also occasionally reported for these negative ΔH amorphous alloys.[59] Either clustering or ordering helps to stabilize the amorphous structure by reducing the enthalpy and hence the free energy of the amorphous phase. As a result, such an amorphous phase is often stabilized to a rather low-energy state, with the heat of crystallization typically of the order of only a few kJ/mol.[60,61] The amorphous structure is often more energetically favorable than the competing crystalline solid-solution phase and forms relatively readily in nonequilibrium processing.[60,61] In this regard, the Ag-Cu amorphous phase appears to be different. It forms not because it has a lower energy than the competing fcc supersaturated solution, but because of kinetic trapping at very high quench rates that keeps it form crystallizing. The fcc phase in fact has a lower enthalpy and a lower free energy at low temperatures, as seen in Fig. 2. In this Ag-Cu case, the amorphous phase is largely homogeneous, and the reduction in energy has to arise from topological local order with little extra contribution from short-range ordering or segregation. This may have contributed to the relatively low stability of the amorphous Ag-Cu phase. Reducing the quench rate would facilitate the development of local structures to help stabilize the amorphous Ag-Cu; however, as shown in Figs. 1, 2, and 4, while slower cooling indeed makes chemical partitioning possible, it also alleviates the kinetic constraints that suppresses the crystallization of the undercooled liquid into the crystalline solution, allowing the latter to replace the amorphous phase at increasingly higher temperatures.

B. Crystalline solutions

Figure 4 suggests that a rapid quench at an effective cooling rate of approximately $5 \times 10^{11} - 5 \times 10^{12}$ K/s would allow the phase decomposition to be bypassed in the undercooled liquid. These quench rates, however, are no longer able to suppress the polymorphous crystallization observed in Fig. 2. This latter transition occurs at a fairly low temperature for these relatively high quench rates. The resulting fcc solid solution is by and large homogeneous. Crystallization becomes possible at higher temperatures with decreasing quench rates. When the quench is slowed down to 2×10^{11} K/s, phase separation sets in almost concurrently with crystallization (compare Figs. 2 and 4). Slowing down the quench further to 5×10^{10} K/s enables the compositional partitioning to occur at still higher temperatures before the crystallization event. The different temperature dependence is understandable by comparing the kinetics of the two processes: the easier polymorphous crystallization has a lower activation energy than that of chemical segregation. Note that once composition modulations (Ag-rich and Cu-rich regions) are developed to sufficiently large dimensions in the undercooled liquid, crystallization of the inhomogeneous alloy is easier and likely to immediately follow, as observed in Fig. 2.

Once crystallization is over, it appears that there is insignificant further development of partitioning inside the fcc solution, as suggested by the more or less constant CSRO parameter after the jumps in Fig. 4. At first glance this would seem to be inconsistent with the equilibrium phase diagram, which indicates that the fcc state would have a stronger tendency to phase separate than the liquid state.[1] Indeed, at the eutectic temperature of 1053 K there is a miscibility gap in the solid, but not in the liquid. The calculated critical temperature of the fcc miscibility gap is at 1385 K,[2] higher than that of the liquid miscibility gap. Clearly, there is a larger positive ΔH in the fcc state due to the size mismatch (13%) between the two elements and hence the strain energy associated with forming the regular lattice. However, the composition profiles inside the fcc solution can be retained due to kinetic constraints, more so than for the undercooled liquid. The clustering kinetics inside a crystalline structure at low temperatures significantly below the critical temperature will be a lot slower than in the undercooled liquid at higher temperatures above the glass transition temperature.

Over a range of quench rates of approximately $5 \times 10^{10} - 5 \times 10^{11}$ K/s, the product crystalline solution is inho-

mogeneous. The partially decomposed regions, as estimated from Fig. 8 with a two-dimensional cut of the atomic configuration, have dimensions as small as fine as a couple of nanometers (modulation wavelength less than a few nanometers). Similar spinodal decomposition features with modulation wavelengths of 1–3 nm have been observed before in annealed Au-Ni,[62–64] a system with an atomic-size mismatch similar to the Ag-Cu case.

C. Comparison with laboratory experiments

None of the experiments on the Ag-Cu system reported in literature explored in a systematic way the atomic-level structures and the homogeneity of the nonequilibrium alloy produced.[3–18] A meaningful comparison is therefore not possible at this point. We have started a series of systematic experiments, and the results will be reported in a forthcoming publication.

Note that all our MD quench experiments started from the liquid phase. While it is possible that during vapor quench the material may indeed go through the liquid temperature range, caution should be exercised if one is to compare directly our results with vapor deposition experiments. Our results cannot be directly applied to those melt quench experiments either because they typically have slower effective cooling rates. However, we believe that the trend of structural evolution towards the fcc solution and towards inhomogeneity with decreasing quench rates should be present in samples prepared in laboratory experiments. Over the three decades of quench rates employed in this study, our MD results suggests three regimes. At the high end above 5×10^{12} K/s, a homogeneous amorphous solution is obtained. Such a rate is difficult to reach in laboratory experiments except in limited vapor deposition conditions.[6–9] The slower quenches at rates over the next decade until 5×10^{11} K/s produces crystalline alloys instead, but retains the homogeneity inside the alloy. Such rates are more likely in vapor deposition experiments, such that some of the experiments may indeed have resulted in single-phase, uniform, Ag-Cu supersaturated solutions.[49] However, if the effective quench rate is reduced by another order of magnitude to between 5×10^{11} and 5×10^{10} K/s, the fcc solutions obtained can be only "x-ray homogeneous," but actually nonuniform. This is a strong possibility for many reported Ag-Cu solutions since they were prepared by procedures that are unlikely to yield sufficiently high quench rates (although a one-to-one correspondence with MD quench rates is not appropriate). So far, they have not been scrutinized carefully to detect (incipient) decomposition.

For quench rates below 5×10^{10} K/s, MD simulations become impractical at present. It is likely that crystallization occurs at a temperature higher than the critical temperature such that the undercooled liquid does not get to enter the miscibility gap. In this case, all the decomposition has to proceed in the crystalline state. We have shown in Fig. 4 that the development of local clustering is slower in the crystalline solution than in the undercooled liquid. However, considering the fairly low quench rate often used in melt quench experiments [down to 10^6 K/s (Ref. 55)] and hence much

longer diffusion times available during the quench than the cases in Fig. 4, it is possible that phase decomposition would also become gradually more and more pronounced in the crystalline alloy. The early stage of spinodal decomposition, often proceeding in a coherent or semicoherent manner, could have easily escaped detection since the alloys have only been analyzed using diffraction methods.[28]

We stress again that the MD results only provide insight into the trend of structural evolutions, while the exact quench rates at which structural changes occur may be dependent on MD details such as the algorithms, the interatomic potentials, and the system size and thus may differ from experimental findings. In fact, from the experimental perspective, it is also difficult to assign a precise effective quench rate to a given set of experimental deposition/quench parameters. Nevertheless, it is well known that a wide range of effective quench rates including those comparable to what have been used in this MD work is possible through the choice of processing techniques and parameters. Typical rapid quench methods at our disposal are melt quenching, laser quenching, evaporation, sputter deposition, ion implantation, and ion beam mixing.[55]

We also note that we used a relatively small simulation cell (2000 atoms) to speed up MD runs and facilitate data analysis. Although the periodic boundary condition may hinder the evolution of the spinodal decomposition by suppressing the long-wavelength fluctuations, the main clustering and decomposition features we are interested in are on the scale of 1 nm and would thus remain observable, and were indeed observed. Due to the rapid and deep quench used, long-range diffusional spinodal decomposition with large wavelengths do not get to develop and small wavelength modulations dominate. In fact, we knew *a priori* from preliminary extended x-ray absorption fine structure (EXAFS) and small-angle x-ray scattering experiments in rapidly quenched Ag-Cu as well as in Ag-Ni (see Sec. IV A) that the main phase separation features would have modulations of the order of only a couple of nanometers. In the design of MD cells, as shown in Fig. 8, we decided to choose to have one dimension (1D) much longer (up to about 8 nm) than the others to allow us the possibility to observe longer-wavelength fluctuations at least in 1D, if they do develop.

Similar to most published MD work, we repeated a few runs with different starting configurations for each MD quench experiment. The limited number of chemical complexions probed may limit the chances of the structure to evolve away from certain metastable frozen states to further lower its energy. Note, however, that we are interested in establishing a trend toward decomposition when different quench conditions are compared, not all the possible states the solutions could reach, or the solution structure that definitely has the lowest energy among all possible complexions, or an accurate determination of the free energy or ordering parameter. Therefore, a limited number of chemical complexions should be sufficient to at least show us the high-probability events and the general tendency. Also note that in the real-world rapid quench experiments kinetics are also extremely limited and metastable frozen structures are actually what people often observe after the quench.

Our MD modeling results will be useful in supplementing the experimental investigations currently underway in our laboratory using probes sensitive to fine-scale structures such as extended x-ray absorption fine structure and small-angle x-ray scattering. A combined simulation-experiment approach will be required to fully understand the nature of the structures of these unconventional supersaturated alloys prepared under a wide range of different far-from-equilibrium conditions.

V. SUMMARY AND CONCLUDING REMARKS

This MD study is aimed at uncovering the atomic-level structures of the Ag-Cu alloys obtained through rapid quenching at extreme cooling rates. It is designed to provide insight into what kind of alloys are produced and the extent of nanoscale inhomogeneity that is possibly present in such unstable positive ΔH alloys created far from equilibrium. The main conclusions are as follows.

(i) Our MD simulations indicate that amorphous alloys can be formed in the positive ΔH Ag-Cu system. The effective quench rates required are extremely high that they may be achievable only under carefully controlled vapor deposition conditions. This may explain why amorphous Ag-Cu is only seen so far in a couple of thin-film deposition experiments.

(ii) The amorphous phases formed via such extremely rapid quenching are homogeneously alloyed on the atomic level, with little or only slight chemical segregation. This is attributed to the fact that the metastable liquid miscibility gap does not appear until a relatively low temperature not much higher than the glass transition temperature, allowing a quench at sufficiently rapid cooling rate to bypass the decomposition.

(iii) While chemically homogeneous, significant topological short-range order develops in the amorphous Ag-Cu. The icosahedral packing is favored due to the tendency for dense random packing and hence energy reduction. Our data suggest that such local icosahedral ordering can occur in positive ΔH binary amorphous alloys and even under the severe quench conditions used to retain the amorphous structures.

(iv) At moderately reduced effective quench rates comparable to those experienced in typical vapor deposition experiments, the undercooled Ag-Cu liquid transforms to the lower-energy supersaturated crystalline solid-solution state. For a range of quench rates, phase separation remains suppressed in both the undercooled liquid and crystallized states, leading to a close to homogeneous solution as a result of a more or less polymorphous crystallization transformation.

(v) At further reduced cooling rates, including those used in many vapor deposition conditions that are customarily presumed to produce homogeneous alloys, spinodal decomposition in the undercooled liquid can no longer be suppressed upon temperature excursions into the metastable liquid miscibility gap. The ensuing crystallization results in fcc solutions containing composition modulations on the nanometer scale and a positive chemical short-range order parameter.

(vi) Our results point to the need for a careful experimental study of the local structures and homogeneity of the Ag-Cu solutions and similar positive ΔH alloys, including those produced under vapor deposition conditions that have been taken for granted for years to produce homogeneous nonequilibrium alloys. Such studies are even more necessary for the fcc solutions formed under less severe quench conditions (e.g., melt quenching) that are not accessible in current MD simulations.

*Electronic address: ema@jhu.edu

[1] *Binary Alloy Phase Diagrams*, edited by T. B. Massalski (ASM, Metals Park, OH, 1986), Vol. 1, p. 29.

[2] J. L. Murray, Metall. Trans. A **15**, 261 (1984).

[3] P. Duwez, R. H. Willens, and W. Klement, J. Appl. Phys. **31**, 1136 (1960).

[4] R. K. Linde, J. Appl. Phys. **37**, 934 (1966).

[5] S. Nagakura, S. Toyama, and S. Oketani, Acta Metall. **14**, 73 (1967).

[6] S. Mader, A. S. Nowick, and H. Widmer, Acta Metall. **15**, 203 (1967).

[7] S. Mader and A. S. Nowick, Acta Metall. **15**, 215 (1967).

[8] C. N. J. Wagner, T. B. Light, N. C. Halder, and W. E. Lukens, J. Appl. Phys. **39**, 3690 (1968).

[9] C. N. J. Wagner, J. Vac. Sci. Technol. **6**, 650 (1969).

[10] B. Cantor and R. W. Cahn, Scr. Metall. **10**, 381 (1976); Acta Metall. **24**, 845 (1976).

[11] B. Y. Tsaur and J. W. Mayer, Appl. Phys. Lett. **36**, 823 (1980).

[12] L. C. Wei and R. S. Averback, J. Appl. Phys. **81**, 613 (1997).

[13] K. Uenishi, K. F. Kobayashi, K. Y. Ishihara, and P. H. Shingu, Mater. Sci. Eng., A **134**, 1342 (1991).

[14] R. Najafabadi, D. J. Srolovitz, E. Ma, and M. Atzmon, J. Appl. Phys. **74**, 3144 (1993).

[15] T. Klassen, U. Herr, and R. S. Averback, Acta Mater. **45**, 2921 (1997).

[16] F. Wu, P. Bellon, A. J. Melmed, and T. Lusby, Acta Mater. **49**, 453 (2001).

[17] Z. H. Barber, Vacuum **41**, 1102 (1990).

[18] N. Saunders and A. P. Miodownik, J. Mater. Sci. **22**, 629 (1987).

[19] C. Michaelson, C. Gente, and R. Bormann, J. Appl. Phys. **81**, 6024 (1997).

[20] C. Gente, M. Oehring, and R. Bormann, Phys. Rev. B **48**, 13 244 (1993).

[21] H. Rizzo, T. Zocco, T. B. Massalski, and M. Nastasi, Metall. Trans. A **24**, 1027 (1993); **25**, 1579 (1994).

[22] H. Y. Bai, C. Michaelsen, C. Gente, and R. Bormann, Phys. Rev. B **63**, 064202 (2001).

[23] R. Busch, F. Gartner, C. Borchers, P. Haasen, and R. Bormann, Acta Metall. Mater. **43**, 3467 (1995).

[24] R. Busch, F. Gartner, C. Borchers, P. Haasen, and R. Bormann,

Acta Metall. Mater. **44**, 2567 (1996).

[25] C. L. Chien, S. H. Liou, D. Kofalt, W. Yu, T. Egami, and T. McGuire, Phys. Rev. B **33**, 3247 (1986).

[26] J. R. Childress and C. K. Chien, Phys. Rev. B **43**, 8089 (1991).

[27] C. Michalson, C. Gente, and R. Bormann, J. Mater. Res. **12**, 1463 (1997).

[28] C. Michaelsen, Philos. Mag. A **72**, 813 (1995).

[29] L. C. Chen and F. Spaepen, Nature (London) **336**, 366 (1988); Mater. Sci. Eng., A **133**, 342 (1991).

[30] (a) A. Sadoc, Y. Calvayrac, A. Quivy, M. Harmelin, and A. M. Flank, J. Non-Cryst. Solids **65**, 109 (1984); (b) E. Ma and M. Atzmon, J. Alloys Compd. **194**, 235 (1993).

[31] Ch. Hausleitner and J. Hafner, Phys. Rev. B **45**, 128 (1992); R. G. Della Valle, D. Gazzillo, and R. Frattini, and G. Pastore, *ibid.* **49**, 12 625 (1994).

[32] J. Weismueller, J. Non-Cryst. Solids **142**, 70 (1992).

[33] W. Sinkler, C. Michaelsen, and R. Bormann, Phys. Rev. B **55**, 2874 (1997); R. Bormann, Mater. Sci. Eng., A **178**, 55 (1994).

[34] J. H. He, H. W. Sheng, P. J. Schilling, C.-L. Chien, and E. Ma, Phys. Rev. Lett. **86**, 2826 (2001).

[35] J. H. He, H. W. Sheng, and E. Ma, Appl. Phys. Lett. **78**, 1343 (2001).

[36] J. H. He and E. Ma, Phys. Rev. B **64**, 144206 (2001).

[37] H. Jónsson and H. C. Anderson, Phys. Rev. Lett. **22**, 2295 (1988); A. S. Clarke, and H. Jónsson, Phys. Rev. E **47**, 3975 (1993).

[38] F. Yonezawa, Solid State Phys. **45**, 179 (1991).

[39] S. Cozzini and M. Ronchetti, Phys. Rev. B **53**, 12 040 (1996).

[40] D. Nelson and F. Spaepen, Solid State Phys. **42**, 1 (1989).

[41] Y. Qi, T. Cagin, W. L. Johnson, and W. A. Goddard, J. Chem. Phys. **115**, 385 (2001).

[42] A. P. Sutton and J. Chen, Philos. Mag. Lett. **61**, 139 (1990); H. Rafii-Tabar and A. P. Sutton, *ibid.* **63**, 217 (1991).

[43] M. Parrinello and A. Rahman, Phys. Rev. Lett. **45**, 1196 (1980); J. Appl. Phys. **52**, 7182 (1981).

[44] S. Nosé, Mol. Phys. **2**, 255 (1984).

[45] (a) R. M. Wentzcovitch, Phys. Rev. B **44**, 2358 (1991); (b) M. P. Allen and D. J. Tildesley, *Computer Simulation of Liquids* (Oxford University Press, New York, 1987).

[46] H. W. Sheng and E. Ma, Phys. Rev. B **61**, 9979 (2000).

[47] G. Mazzone, V. Rosato, and M. Pintore, Phys. Rev. B **55**, 837 (1997).

[48] H. W. Sheng and E. Ma, Phys. Rev. B **63**, 224205 (2001).

[49] H. W. Sheng, G. Wilde, and E. Ma, Acta Mater. **50,** 475 (2002).

[50] Richard Zallen, *The Physics of Amorphous Solids*, (Wiley-Interscience, New York, 1983).

[51] Y. Qi, T. Cagin, Y. Kimura, and W. A. Goddard III, Phys. Rev. B **59**, 3527 (1999).

[52] B. E. Warren, B. L. Averbach, and B. W. Robert, J. Appl. Phys. **22**, 1493 (1951).

[53] T. Takagi, T. Ohkubo, Y. Hirotsu, B. S. Murty, K. Hono, and D. Shindo, Appl. Phys. Lett. **79**, 485 (2001).

[54] J. Saida, M. Matsushita, and A. Inoue, Appl. Phys. Lett. **79**, 412 (2001).

[55] M. Ohring, *The Materials Science of Thin Films* (Academic, San Diego, 1992), p. 235.

[56] H. Ikeda, Y. Qi, T. Cagin, K. Samwer, W. L. Johnson, and W. A. Goddard III, Phys. Rev. Lett. **82**, 2900 (1999).

[57] *Binary Alloy Phase Diagrams*, edited by T. B. Massalski (American Society for Metals, Materials Park, OH, 1986), p. 65.

[58] W. K. Luo and E. Ma (unpublished).

[59] F. Gartner, C. Michaelsen, and R. Bormann, Philos. Mag. **76**, 511 (1997).

[60] W. L. Johnson, Prog. Mater. Res. **30**, 81 (1986); MRS Bull. **24**, 42 (1999).

[61] A. Lindsay Greer, Science **267**, 1947 (1995), and references therein.

[62] J. W. Cahn, in *The Selected Works of John W. Cahn*, edited by W. C. Carter and W. C. Johnson (TMS, Warrendale, PA, 1998), p. 1.

[63] W. M.-C. Yang, Ph.D. thesis, Northwestern University, 1970.

[64] F. Hofer and P. Warbichler, Z. Metallkd. **76**, 11 (1985).